

Heat Transfer From Radiatively Heated Material in a Low Reynolds Number Microgravity Environment

H. Yamashita¹

H. R. Baum

G. Kushida¹

K. Nakabe²

T. Kashiwagi

Building and Fire Research Laboratory,
National Institute of Standards and
Technology,
Gaithersburg, MD 20899

A mathematical model of the transient three-dimensional heat transfer between a slowly moving ambient gas stream and a thermally thick or thin flat surface heated by external radiation in a microgravity environment is presented. The problem is motivated in part by fire safety issues in spacecraft. The gas phase is represented by variable property convection-diffusion energy and mass conservation equations valid at low Reynolds numbers. The absence of gravity and low Reynolds number together permit the flow to be represented by a self-consistent velocity potential determined by the ambient velocity and the thermal expansion in the gas. The solid exchanges energy with the gas by conduction/convection and with the surroundings by surface absorption and re-emission of radiation. Heat conduction in the solid is assumed to be one dimensional at each point on the surface as a consequence of the limited times (of order of 10 seconds) of interest in these simulations. Despite the apparent simplicity of the model, the results show a complex thermally induced flow near the heated surface. The thermal exchange between the gas and solid produces an outward source-like flow upstream of the center of the irradiated area and a sink-like flow downstream. The responses of the temperature fields and the associated flows to changes in the intensity of the external radiation and the ambient velocity are discussed.

1 Introduction

This paper is a continuation of our analysis of heat transfer phenomena associated with the radiative ignition of cellulosic materials in a microgravity environment. The objective of this work is both scientific understanding and the development of a potential hazard analysis capability for spacecraft fire safety studies. The use of a microgravity environment to study radiative ignition eliminates the need to study simultaneously the starting buoyant plume, which is itself a major task requiring a time-dependent solution to multidimensional Navier-Stokes equations. Previous radiative auto-ignition models avoided this problem by limiting the analysis to one dimension (Kashiwagi, 1974; Kindelan and Williams, 1977; Baek and Kim, 1991), or at a stagnation point (Amos and Fernandez-Pello, 1988). Almost any scenario of interest in a spacecraft potential hazard analysis is both multidimensional and time dependent. Thus, one of the goals of the present work is a formulation of a computationally tractable model of the thermal transport that can be used in transient three-dimensional ignition studies.

In a microgravity environment, the dominant vorticity creation mechanism in the bulk of the gas is absent. Vorticity is still generated at the surface by the non-slip condition. However, at low Reynolds numbers the tangential velocity profile near the surface is not important in the convective transport of mass, momentum, or energy. Thus, the no-slip condition was relaxed in our earlier study of radiatively induced degradation of a thermally thin solid in a quiescent gas (Kushida et al., 1992). This permitted the flow in this axially symmetric configuration to be represented by a velocity potential. In the present work, this approximation is used to investigate two major extensions; the incorporation of a slow ambient flow generalizing the analysis to three dimensions, and coupling this to both thermally thick and thermally thin solid samples. These extensions are motivated by the experimentally observed strong

effects of ambient flow velocity on flame spread rate in a microgravity environment (Olson et al., 1988; Olson, 1991). It appears that a ventilation flow in a spacecraft should have a strong effect on the flame spread rate. In the present study only the coupled heat transfer processes are studied. Later papers will describe the effects of the condensed phase degradation reactions and gas phase oxidation.

2 Theory

2.1 Gas Phase. The study of radiative heating or ignition of solid fuels in a microgravity environment requires a description of time-dependent coupled processes in both the gas and solid phases. The mathematical and computational complexity inherent in such a study suggests that the simplifications permitted by the microgravity environment and the small physical scale of the idealized experiment be built into the mathematical model. These simplifications principally affect the gas phase processes. The absence of gravity removes the buoyancy-induced vorticity generation mechanism. The small radiatively heated surface area in the scenarios of interest together with the slow externally imposed velocity implies a low Reynolds number flow domain. Classical analyses of low Reynolds number flows have demonstrated that using the Oseen approximation to the convective terms in the equations of motion "constitutes an ad-hoc uniformization" (Van Dyke, 1964) of the first approximation to the rigorous calculation of the flow past isolated bodies. The central point that emerges from these analyses is that diffusion dominates convection near the surface, so the fact that the Oseen flow does not satisfy the no-slip boundary condition is irrelevant at lowest order in the theory. When the gasification of condensed fuels is included in our future studies, the thermally induced surface blowing velocity must be taken into account, even at low Reynolds numbers. The generalization to a flow past an arbitrarily shaped body with a prescribed surface blowing distribution can also be accommodated by a potential flow, if vorticity generated in the interior of the flow is not significant.

The potential flow description of the velocity field greatly simplifies both the formulation and subsequent computation

¹Guest researcher from Nagoya University, Nagoya, Japan.

²Guest researcher from Osaka University, Osaka, Japan.

Contributed by the Heat Transfer Division for publication in the JOURNAL OF HEAT TRANSFER. Manuscript received by the Heat Transfer Division March 1992; revision received November 1992. Keywords: Microgravity Heat Transfer, Transient and Unsteady Heat Transfer. Associate Technical Editor: L. S. Fletcher.

of a wide variety of low Reynolds number microgravity heat transfer and combustion problems. Accordingly, the formulation will be developed in a fairly general context and then specialized to the specific case of the radiative heating of a thermally thick solid. The starting point is the conservation of mass and energy in the gas. Under low Mach number heat transfer conditions, generalized governing equations including gas phase oxidation reactions and radiative heat transfer can be written as:

$$\frac{D\rho}{Dt} + \rho \nabla \cdot \mathbf{v} = 0 \quad (1)$$

$$\rho c_p \frac{DT}{Dt} - \nabla \cdot (k \nabla T) = \dot{q}_R(\mathbf{r}, t) \quad (2)$$

Here, $\dot{q}_R(\mathbf{r}, t)$ is the net chemical and radiative heat release per unit volume into the gas of density ρ , temperature T , and velocity \mathbf{v} . The gas was assumed to be air. The specific heat c_p and thermal conductivity k are in general functions of T , and they are fitted by the fifth-order polynomial expression. These equations are supplemented by an equation of state, taken in a form appropriate for low Mach number flows:

$$\rho h = \rho_\infty h_\infty \quad (3)$$

The subscript ∞ refers to suitable ambient or reference conditions:

$$h = \int_0^T c_p(T) dT \quad (4)$$

Now multiply Eq. (1) by h and add it to Eq. (2). The result, after using Eqs. (3) and (4), is:

$$\rho_\infty h_\infty \nabla \cdot \mathbf{v} - \nabla \cdot (k \nabla T) = \dot{q}_R(\mathbf{r}, t) \quad (5)$$

Equation (5) is the fundamental equation for determining the velocity field \mathbf{v} . Since \mathbf{v} is a vector field, it can be decomposed into the gradient of a potential ϕ and a solenoidal field \mathbf{u} :

$$\mathbf{v} = \nabla \phi + \mathbf{u} \quad (6)$$

$$\nabla \cdot \mathbf{u} = 0 \quad (7)$$

Substitution of Eqs. (6) and (7) into Eq. (5) yields:

$$\nabla^2 \phi = \frac{1}{\rho_\infty h_\infty} (\dot{q}_R(\mathbf{r}, t) + \nabla^2 \psi) \quad (8)$$

$$\psi = \int_{T_\infty}^T k(T) dT \quad (9)$$

Note that the second term on the right-hand side of Eq. (8) can be eliminated by introducing a particular solution ϕ_p as:

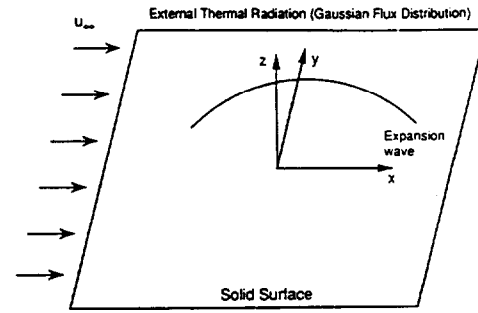


Fig. 1 A schematic illustration of coordinates and the flow field near the heated surface area by external radiation

$$\phi_p = \frac{\psi}{\rho_\infty h_\infty} \quad (10)$$

Furthermore, it is convenient to introduce another particular potential $\phi_{p\infty}$ representing the effect of the ambient wind velocity u_∞ . Then, introducing a remainder of potential $\Phi(\mathbf{r}, t)$, ϕ may be expressed in the form:

$$\phi = \phi_p + \phi_{p\infty} + \Phi(\mathbf{r}, t) \quad (11)$$

$$\nabla^2 \Phi = \frac{\dot{q}_R(\mathbf{r}, t)}{\rho_\infty h_\infty} \quad (12)$$

Equations (10), (11), and (12) relate the potential field to the temperature distributions in the gas phase. Since it is necessary to determine this quantity in any event, solution of Eq. (12) represents the minimum additional work required to obtain a self-consistent velocity field. Implied in this statement is the assumption that the solenoidal velocity field \mathbf{u} is not of interest in its own right. If \mathbf{u} is of interest, then there is no alternative to solving the Navier-Stokes equations. However, a large portion of both the combustion and heat transfer literature consists of calculations in which the details of the velocity field are approximated, often crudely, in order to understand the thermophysical phenomenon of direct interest. In the present circumstances, the approximations have been justified in simple geometries by detailed analyses, and interest will be confined to temperature fields induced by radiative heating.

Now consider the specific problem of heat transfer from radiative heating of thermally thick solid with a slow flow along the surface in microgravity environment. The geometry is shown in Fig. 1. Let x , y , and z be the streamwise, spanwise, and transverse coordinates in a three-dimensional Cartesian coordinate system as shown in the figure. The center of the

Nomenclature

c, c_p = specific heat
 G = Green's function
 h = enthalpy
 k = thermal conductivity
 Pe = Peclet number
 $Pe_i = 1/Pe$
 \dot{q} = heat flux
 \dot{q}_N = net heat flux at solid surface
 \dot{q}_R = net chemical and radiative heat release in the gas phase
 r, \mathbf{r} = distance from origin, position vector
 r_0 = width of Gaussian distribution of external radiation

T = temperature
 t = time
 \mathbf{u} = solenoidal velocity vector
 u_∞ = ambient velocity
 \mathbf{v} = velocity vector
 x, y, z = Cartesian coordinates (streamwise, spanwise, transverse)
 α = thermal diffusivity
 δ = thickness of thin solid sheet
 ϵ = emissivity
 Δt = time interval
 $\Delta x, \Delta y, \Delta z$ = grid spacing
 ρ = density

σ = Stefan-Boltzmann constant
 Φ = remainder potential function
 ϕ = potential function
 ϕ_p = particular solution of potential function
 ψ = potential function related with heat conduction

Subscripts

N = net
 rad = solid surface re-radiation
 s = solid phase
 ∞ = ambient or reference condition

concentrated external radiant flux with a Gaussian distribution impinging on the solid surface is set up at the origin of coordinates. The ambient flow is parallel to the solid surface and then $\phi_{p\infty} = u_{\infty}x$. The gas is assumed to be transparent to the radiation. Under these circumstances, the term $\dot{q}_R(r, t)$ in Eq. (2) can be ignored. The gas phase energy conservation equation takes the form:

$$\rho c_p \left(\frac{\partial T}{\partial t} + \mathbf{v} \cdot \nabla T \right) = \nabla \cdot (k \nabla T) \quad (13)$$

This equation is to be solved together with Eqs. (10), (11), and (12), subject to boundary and initial conditions.

At time $t = 0$, the entire system is assumed to have uniform flow at ambient temperature T_{∞} . Hence:

$$\begin{aligned} \Phi(x, y, z, 0) &= 0 \\ T(x, y, z, 0) &= T_{\infty} \end{aligned} \quad (14)$$

Once the heating process has started, the temperature at the solid surface $T_s(x, y, 0, t)$ rises above ambient, and the temperatures at the flow inlet and open boundaries remain at T_{∞} . The gas phase boundary conditions for temperature and Φ must be provided at the flow inlet $x = -\infty$ and the flow exit $x = +\infty$, at the symmetric boundary $y = 0$, at the open boundary $y = \infty$ and $z = \infty$, and at the solid surface $z = 0$. The boundary conditions for temperature T can be expressed as follows:

$$\begin{aligned} T(\pm\infty, y, z, t) &= T_{\infty} \\ \frac{\partial T(x, 0, z, t)}{\partial y} &= 0 \\ T(x, \infty, z, t) &= T_{\infty} \\ T(x, y, 0, t) &= T_s(x, y, 0, t) \\ T(x, y, \infty, t) &= T_{\infty} \end{aligned} \quad (15)$$

The boundary conditions for Φ are:

$$\begin{aligned} \Phi(-\infty, y, z, t) &= \Phi_{x-\infty} \\ \Phi(\infty, y, z, t) &= \Phi_{x\infty} \\ \frac{\partial \Phi(x, 0, z, t)}{\partial y} &= 0 \\ \Phi(x, \infty, z, t) &= \Phi_{y\infty} \\ \rho_{\infty} h_{\infty} \frac{\partial \Phi(x, y, 0, t)}{\partial z} &= -k \frac{\partial T(x, y, 0, t)}{\partial z} \\ \Phi(x, y, \infty, t) &= \Phi_{z\infty} \end{aligned} \quad (16)$$

where $\Phi_{x-\infty}$, $\Phi_{x\infty}$, $\Phi_{y\infty}$, and $\Phi_{z\infty}$ are the values at positions far away from the solid surface. Far from the surface, Φ and T must decay to their ambient values. Translating this into boundary conditions suitable for numerical computation, however, requires some care. Numerical boundary conditions are applied at the sides of a rectangular box shaped computational domain. Since T decays exponentially to its ambient value, using Eq. (14) is permissible until the first calculated non-ambient contours of these quantities approach the computational boundary. However, the potential field decays slowly away from the heated region, i.e., $\Phi \sim (x^2 + y^2 + z^2)^{-1}$. Thus, putting Φ or its gradient equal to zero at the computational boundary would introduce unacceptable errors into the calculation. These errors can be avoided by using Eq. (17) shown below, that is, the solution to Eq. (12) subject to the boundary condition given by Eq. (16).

$$\begin{aligned} \rho_{\infty} h_{\infty} \Phi &= \int_{-\infty}^{\infty} dx_0 \int_{-\infty}^{\infty} dy_0 \int_0^{\infty} dz_0 \dot{q}_R(x_0, y_0, z_0) G(x, y, z, x_0, y_0, z_0) \\ &+ \rho_{\infty} h_{\infty} \int_{-\infty}^{\infty} dx_0 \int_{-\infty}^{\infty} dy_0 \frac{\partial \Phi(x_0, y_0, 0, t)}{\partial z} G(x, y, z, x_0, y_0, 0) \end{aligned}$$

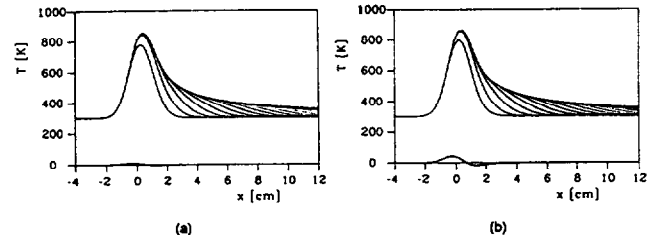


Fig. 2 Time history of surface temperature distribution at $y = 0$ and at the interval of 0.5 s for the case of linear problem ($u_{\infty} = 2$ cm/s, $\dot{q}_0 = 4$ W/cm²) and difference between the analytical solution and the numerically calculated results at 10 s: (a) grid size 128 \times 32 \times 32; (b) grid size 64 \times 16 \times 16

$$G(x, y, z, x_0, y_0, z_0) = -\frac{1}{4\pi} \left(\frac{1}{[(x-x_0)^2 + (y-y_0)^2 + (z-z_0)^2]^{1/2}} + \frac{1}{[(x-x_0)^2 + (y-y_0)^2 + (z+z_0)^2]^{1/2}} \right) \quad (17)$$

G is a Green's function satisfying Neumann boundary conditions. Now $\partial \Phi(x, y, 0, t)/\partial z$ is given by Eq. (16) at any instant of time, and the temperature is an exponentially decaying function of the radial integration variable in Eq. (17). Hence, the use of Eq. (17) to evaluate Φ around the computational boundary provides a fast and highly accurate means of applying computational boundary conditions to Φ .

2.2 Condensed Phase Model. In much of the present paper the sample is thermally thick. Since it is expected that the ignition event would occur within a relatively short time (less than 10 seconds) after the beginning of external irradiation, only heat conduction normal to the surface is important and conduction along the y and x coordinates is assumed to be negligible. Also, it is assumed that the condensed material is opaque and there is no radiative transfer in the sample. Thermal properties of the sample are assumed to be independent of temperature. Then, the governing energy equations for the condensed phase are given as follows:

$$\frac{\partial T_s}{\partial t} = \alpha_s \frac{\partial^2 T_s}{\partial z^2} \quad (18)$$

where α_s is the thermal diffusivity of the solid. The initial condition and the boundary condition are as follows:

$$\begin{aligned} T_s(x, y, z, 0) &= T_{\infty} \\ T_s(x, y, -\infty, t) &= T_{\infty} \end{aligned}$$

$$T_s(x, y, 0, t) = T(x, y, 0, t), \quad k_s \frac{\partial T_s(x, y, 0, t)}{\partial z} = \dot{q}_N \quad (19)$$

Then, the solution for the surface temperature yields the following relation:

$$k_s [T_s(x, y, 0, t) - T_{\infty}] = \int_0^t \left(\frac{\alpha_s}{\pi(t-\tau)} \right)^{1/2} \dot{q}_N(x, y, \tau) d\tau \quad (20)$$

The subscript s refers to properties of the condensed phase, and \dot{q}_N is the net heat flux to the solid surface.

The net heat flux at the material surface is

$$\dot{q}_N = \dot{q}_{ex} - \dot{q}_{rad} + k \frac{\partial T(x, y, 0, t)}{\partial z} \quad (21)$$

where \dot{q}_{ex} is external radiant flux and its distribution is defined to be Gaussian. In the calculation reported here,

$$\dot{q}_{ex} = \dot{q}_0 \exp \left[-\left(\frac{r}{r_0} \right)^2 \right] \quad (22)$$

where $r = (x^2 + y^2)^{1/2}$, $r_0 = 1$ cm and \dot{q}_0 is a peak external radiant flux. \dot{q}_{rad} is the re-radiation flux from the material surface and is given by the following expression:

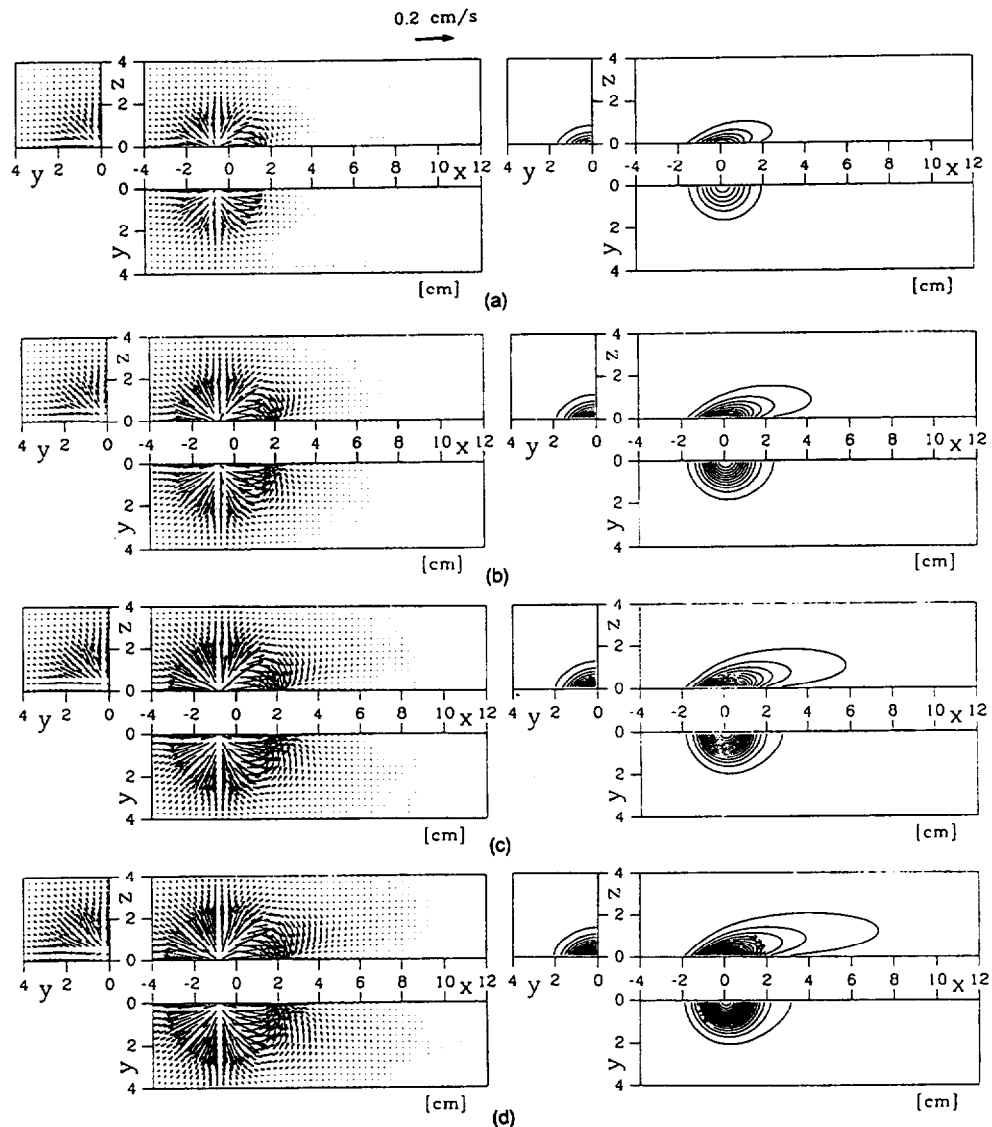


Fig. 3 The distributions of velocity vectors relative to ambient flow and the temperature contours (from 310 K at the interval of 20 K) for $u_\infty = 2$ cm/s and $\dot{q}_0 = 4$ W/cm². (a) $t = 2$ s; (b) $t = 4$ s; (c) $t = 6$ s; (d) $t = 8$ s

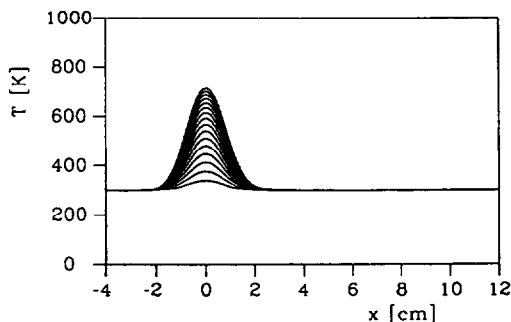


Fig. 4 Time history of the surface temperature distribution at $y = 0$ for $u_\infty = 2$ cm/s and $\dot{q}_0 = 4$ W/cm² at the interval of 0.5 s

$$\dot{q}_{\text{rad}} = \epsilon \sigma [T_s^4(x, y, 0, t) - T_\infty^4] \quad (23)$$

where the Stefan-Boltzmann constant $\sigma = 56.7 \times 10^{-13}$ W/(cm²·K⁴). The surface re-radiation is quite important when the surface temperature becomes high. Therefore, the surface temperature can rise to the value at which re-radiation flux becomes equal to external radiant flux. The surface temperature reaches as high as 919 K or 1091 K for $q_0 = 4$ or 8 W/cm² with $\epsilon = 1.0$ and $T_\infty = 300$ K, respectively.

Two other limiting cases of this heat transfer problem have been studied for comparison purposes; the thermally thin solid with the same gas phase description, and a simplified gas phase heat transfer problem for which an analytical solution can be derived to examine the accuracy of the numerical code. For a thermally thin material, the governing energy equation, Eq. (18), does not need to be solved and the following boundary equation is used:

$$\rho_s c_s \frac{\partial T_s(x, y, 0, t)}{\partial t} \delta = \dot{q}_{\text{ex}} - \dot{q}_{\text{rad}} + k \frac{\partial T(x, y, 0, t)}{\partial z} \quad (24)$$

where δ is the thickness of the thermally thin sheet. Since a cellulosic paper has been used for the thermally thin material in our previous studies (Kushida et al., 1991), the same thermal properties of the cellulosic paper are used.

Heat transfer with an Oseen flow problem is selected to obtain the analytical solution to test the numerical code. The flow field is uniform with u_∞ and only the energy equation in the gas phase is involved as described in the appendix. Heat is transferred by conduction and convection from the specified energy flux at the surface. The analytical solution is derived and expressed as

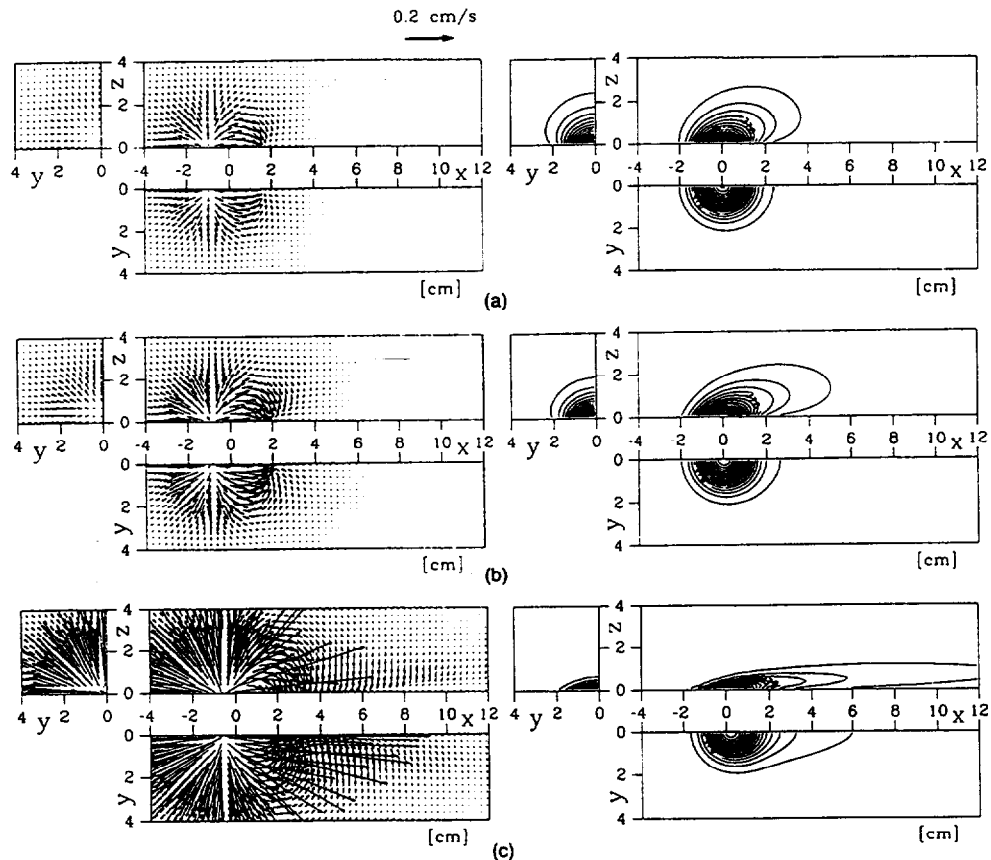


Fig. 5 Effects of ambient flow velocity on the distributions of velocity vectors relative to the ambient flow and the temperature contours (from 310 K at the interval of 20 K) at $t = 8$ s for $\dot{q}_0 = 4$ W/cm². (a) $u_\infty = 0.5$ cm/s ($Pe = 2.27$); (b) $u_\infty = 1.0$ cm/s ($Pe = 4.55$); (c) $u_\infty = 10$ cm/s ($Pe = 45.5$)

$$\theta = \frac{\int_0^7 \sqrt{Pe_i} \exp \left\{ -(\bar{x} - \tau)^2 + (\bar{y})^2 \right\} / (1 + 4Pe_i\tau) - (\bar{z})^2 / 4Pe_i\tau \, d\tau}{\pi^{3/2} \sqrt{\tau} (1 + 4Pe_i\tau)} \quad (25)$$

where θ , \bar{x} , \bar{y} , \bar{z} , \bar{t} are nondimensionalized temperature, three coordinates, and time as defined in the appendix. Pe_i is a reciprocal of a Peclet number, which is $k / (\rho C_p u_\infty r_0)$. The integral in Eq. (25) is calculated numerically and the results are compared with those calculated by a finite difference method. The comparison is shown in the next section.

2.3 Numerical Methods. For the gas phase, the numerical calculation is performed by using a finite difference method. The Gaussian external radiant flux radius r_0 is fixed at 1.0 cm. The computational domain is taken to be $x = -4.8-14.4$ cm, $y = 0-4.8$ cm, and $z = 0-4.8$ cm. Two different grid sizes were used: $128 \times 32 \times 32$ corresponding to a grid spacing $\Delta x = \Delta y = \Delta z = 0.15$ cm and $64 \times 16 \times 16$ with cell size $\Delta x = \Delta y = \Delta z = 0.3$ cm. The equations to be solved for the gas phase are those for the potential function Φ and the temperature T .

The equation for Φ is calculated using the FISHPAK direct solver of the Poisson equation in Cartesian coordinates using the standard seven-point finite difference approximation on a staggered grid (VHS3 package, HS3CRT subroutine). The boundary conditions for Φ are specified at the open boundary by evaluating Eq. (17) at each time step. In the present problem, since there are no volumetric source terms, only the surface integral remains. This can be efficiently handled by "coarse graining" the integrals into clusters of 8×8 cells for the $128 \times 32 \times 32$ grid and 4×4 cells for the $64 \times 16 \times 16$ grid. Each subintegral is then estimated by using the average value

over that portion of the surface, but with the source points of the Green's function evaluated at the centroid of the integrand. This is formally equivalent to the first two terms of the asymptotic expansion of each "coarse graining" subintegral. The errors introduced by this procedure are negligible compared with the discretization errors. The equation for temperature is solved using a second-order central difference scheme for both convection and diffusion terms. The time advance is made by using the DuFort Frankel method with a time interval $\Delta t = 0.01$ s (for Grid $64 \times 16 \times 16$) or $\Delta t = 0.005$ s (for Grid $128 \times 32 \times 32$). These values of time intervals are sufficiently small to ensure that the Courant condition is satisfied.

For the solid phase, the equations of the temperature T also have to be solved. Equation (20) was reduced to nonlinear algebraic equations with the integral being converted to a summation. These nonlinear algebraic equations were solved by using the Newton-Raphson method. In the case of a thin solid, Eq. (24) is solved by using the Euler explicit method. The computation time for the thermally thick case was about 17 seconds per time step on IBM RS6000/550 computer with $128 \times 32 \times 32$ grids.

3 Results and Discussion

3.1 Comparison With the Linear Analytical Solution. The numerically calculated results for the simplified heat transfer model were compared with the analytically calculated results of Eq. (25) for the case of $u_\infty = 2$ cm/s (Peclet number $Pe = u_\infty r_0 / (k / \rho C_p) = 9.1$), $\dot{q}_0 = 4$ W/cm² to examine the accuracy of the numerical method. The results in Figs. 2(a) and 2(b) show the time history of the surface temperature distribution along the x coordinate at the $y = 0$ plane calculated numerically with the two different grid sizes, $128 \times 32 \times 32$ and $64 \times 16 \times 16$, respectively. The bottom of the figures

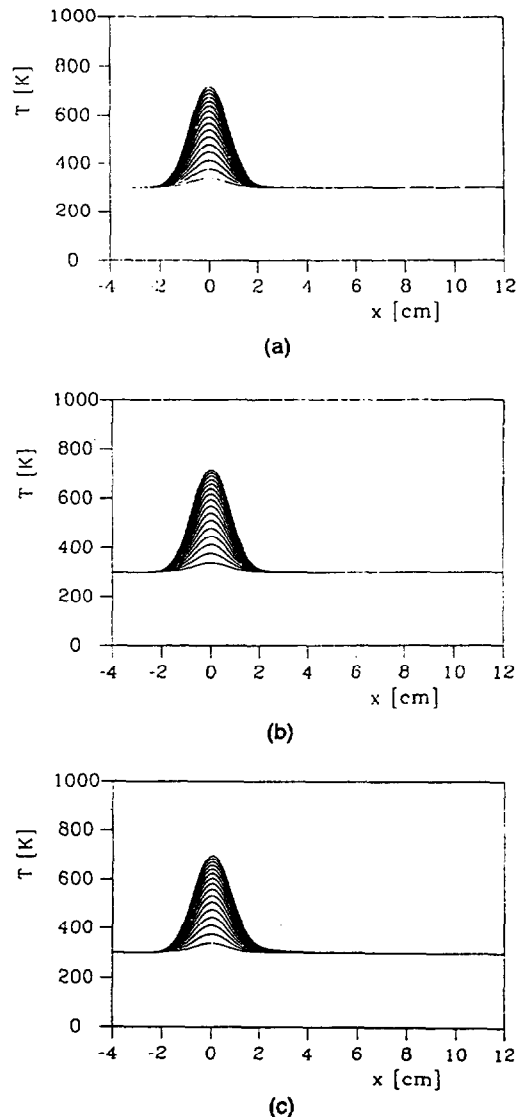


Fig. 6 Time history of surface temperature distributions at $y = 0$ at the interval of 0.5 s for $\dot{q}_0 = 4 \text{ W/cm}^2$: (a) $u_\infty = 0.5 \text{ cm/s}$; (b) $u_\infty = 1.0 \text{ cm/s}$; (c) $u_\infty = 10 \text{ cm/s}$

indicates the difference in surface temperature between the analytical calculation and the numerical calculation. These two figures show that the errors in the numerical calculations are within 1.5 percent for the finer grid size calculation and within 5 percent for the coarser grid size calculation. The rest of the results shown in this paper were obtained using the finer grid size.

3.2 Fluid Flow and Heat Transfer Characteristics. Typical examples of the distributions of velocity vectors relative to ambient flow and temperature contours in the gas phase are shown in Fig. 3 and surface temperature distributions are shown in Fig. 4 for $u_\infty = 2 \text{ cm/s}$ ($Pe = 9.1$), $\dot{q}_0 = 4 \text{ W/cm}^2$, $\epsilon = 1.0$, and the thermally thick solid. Typical values of thermal properties for a plastic (Brandrup and Immergut, 1975) are used for the calculation: $c_s = 1.3 \text{ J/(g}\cdot\text{K)}$, $\rho_s = 1.2 \text{ g/cm}^3$, and $k_s = 2.1 \times 10^{-3} \text{ W/(cm}\cdot\text{K)}$. The arrow indicates the vector projected on each cross section. The length of arrow indicates the magnitude of velocity with the reference value of 0.2 cm/s , and the starting point of arrow indicates the location of velocity vector. The left corner figure in Fig. 3 represents the flow vector distribution in the half of the y plane at $x = 0.075 \text{ cm}$. The top rectangular figure represents the distribution in the x - z plane at $y = 0.075 \text{ cm}$. The lower rectangular figure represents the distribution in the x - y plane at $z = 0.075 \text{ cm}$.

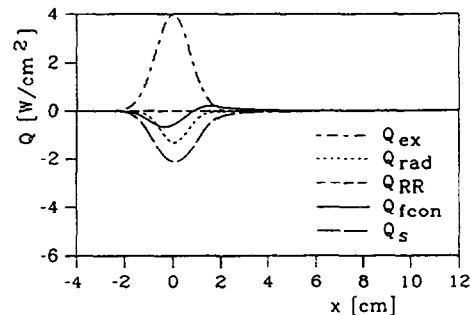


Fig. 7 Energy balance at the surface along $y = 0$ for $u_\infty = 10 \text{ cm/s}$ and $\dot{q}_0 = 4 \text{ W/cm}^2$

The temperature contours are indicated at intervals of 20 K from 310 K. Figures 3(a), 3(b), 3(c), and 3(d) show the results of time $t = 2, 4, 6,$ and 8 s after the irradiation, respectively. The distribution of velocity vectors represents the flow component generated by heat addition from the irradiated surface. This flow is much smaller than the ambient flow of 2 cm/s . There is an upward slow flow generated by the steep temperature gradient due to heat addition. Its center is located a short distance upstream from the center of the external irradiation ($x = 0$). This indicates that the steepest temperature gradient occurs at the upstream location due to downward pushing of the heated layer by the ambient flow. At a short distance downstream from $x = 0$, there is a sink of flow due to the steep temperature gradient resulting from heat loss from the hot gas stream to the cold surface. Since the temperature gradient drives the flow, the flow generated by the external irradiation is limited to a region near the irradiated surface area at an early time. As time increases, the flow velocity gradually increases, but the magnitude of velocity remains at most 0.2 cm/s due to the absence of combustion and buoyancy induced flow. The heated region in the gas phase increases as time increases. The heat in the gas phase is convected radially and downstream by the gas flow due to expansion and ambient flow.

Figure 4 shows the time history of the solid surface temperature distribution $T_s(x, 0, 0, t)$ in the x direction at $t = 0.5 \text{ s}$ intervals. This distribution corresponds to the Gaussian flux distribution of external radiation expressed by Eq. (22) with slight modification by the ambient flow. However, the modification by convective heating is not significant for the results because the ambient flow velocity is small for this case. The temperature increase slows down gradually because of the heat balance between external radiation and the re-radiation loss from the high temperature surface.

3.3 Effects of Parameters on Fluid Flow and Heat Transfer Characteristics. The effects of several parameters, such as ambient flow velocity, external radiant flux, condensed phase thickness, and others, on distributions of velocity vector and temperature in the gas phase were studied. The results are discussed in this section.

3.3.1 Effect of Ambient Flow Velocity, u_∞ . Figures 5(a), 5(b), and 5(c) show the distributions of velocity vectors relative to ambient flow and the temperature contours for the three different ambient flow velocities of $u_\infty = 0.5 \text{ cm/s}$ ($Pe = 2.27$), 1.0 cm/s (4.55), and 10.0 cm/s (45.5), respectively. These results are at 8 seconds after the irradiation. The temperature contours are plotted at intervals of 20 K from 310 K. As the ambient flow velocity increases, the heated area is pushed toward the surface and temperature gradients in the gas phase near the surface become steeper. Steeper temperature gradients generate larger flow velocities, as shown in Fig. 5. The center of the heat-generated flow near the surface moves closer to the center of the irradiated area with an increase in the ambient flow velocity. The distributions of surface temperature along

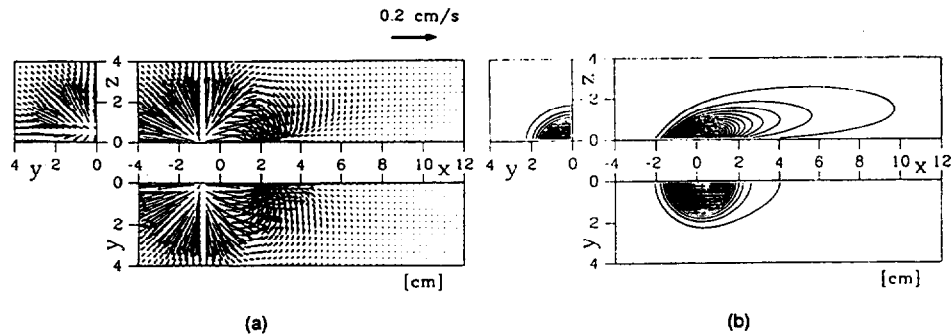


Fig. 8 (a) The distributions of velocity vectors relative to ambient flow, and (b) the temperature contours (from 310 K at the interval of 20 K) for $\bar{q}_0 = 8 \text{ W/cm}^2$ and $u_\infty = 2 \text{ cm/s}$ at 8 s

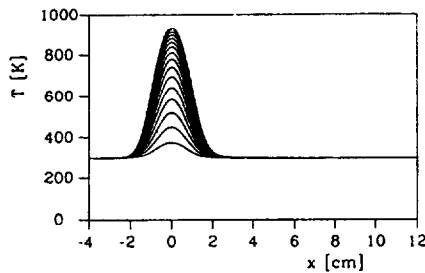


Fig. 9 Time history of surface temperature distribution at $y = 0$ for $\bar{q}_0 = 8 \text{ W/cm}^2$ and $u_\infty = 2 \text{ cm/s}$ at the interval of 0.5 s

$y = 0$ corresponding to the above three cases are shown in Fig. 6. There is no significant difference in surface temperature in the upstream part ($x \leq 0$). The difference occurs only in the downstream region, particularly, where the distribution of surface temperature becomes close to the ambient such as around 2 cm in the case of $u_\infty = 10.0 \text{ cm/s}$.

The energy balance at the surface along $y = 0$ is calculated at 8 seconds and the results are plotted in Fig. 7. The term Q_{ex} is external radiant flux, which is a Gaussian shape as described previously. Q_{rad} is re-radiation loss from the surface, Q_{RR} is the net of thermal degradation reactions that are not included in this study, Q_{con} is convective heating to the surface, and Q_c is heat conduction loss to the interior of the material. The largest heat loss term at this time is the heat conduction loss followed by re-radiation loss. The convection term is negative in the region about $-2 \text{ cm} < x < 0.8 \text{ cm}$ due to higher surface temperatures than gas temperatures. However, in the region about $0.8 \text{ cm} < x < 4 \text{ cm}$ the convective heating term becomes positive due to higher gas temperatures than surface temperatures. This transition in convective heating is caused by the ambient flow. The amount of heat convection increases with an increase in the ambient flow velocity. This could be important for the case from the transition from ignition to flame spread with the ambient flow.

3.3.2 Effects of External Radiation Flux. Figure 8 shows the distribution of velocity vector relative to the ambient flow ($u_\infty = 2 \text{ cm/s}$) and of temperature in the gas phase with external radial flux of 8 W/cm^2 at 8 seconds after the irradiation. It is clear that the heated gas region is larger than that at 4 W/cm^2 shown in Fig. 3(d). Subsequently, the flow field generated by the gas heating for 8 W/cm^2 is larger than that for 4 W/cm^2 . The flow toward the surface and toward the $y = 0$ plane in the immediate downstream region of the irradiated area (almost like a flow toward a sink) shown in Fig. 8 is more distinct than that for 4 W/cm^2 . The maximum surface temperature shown in Fig. 9 is about 950 K, which is slightly higher than about 900 K for 4 W/cm^2 . This small increase in surface temperature from 4 W/cm^2 to 8 W/cm^2 is due to an increase in re-radiation loss from the surface as shown in the energy balance at the surface.

3.3.3 Effects of Solid Thickness. Figure 10 shows the velocity distribution and temperature contours at 8 seconds after irradiation of external radiant flux of 4 W/cm^2 with a thermally thin solid with $\rho_s = 0.6 \text{ g/cm}^3$, $c_s = 1.26 \text{ J/(g}\cdot\text{K)}$, and $\delta = 0.025 \text{ cm}$. The ambient flow velocity is 2 cm/s. Figure 11 shows the history of the surface temperature distribution. The comparison of these results with those shown in Fig. 3(d) indicates the effects of the solid thickness. Since heat loss to the interior of the solid by heat conduction is not included for the thermally thin material, the surface temperature rises rapidly and reaches about 920 K compared to roughly 700 K for the thermally thick material. After 7.5 seconds the surface temperature distribution does not change significantly with time. Therefore, more heat is transferred from the surface to the gas phase and the heated region in the gas phase for the thermally thin material is much larger than the thermally thick material. The corresponding flow velocity induced by the heat addition from the thin material is larger than that for the thick material.

4 Conclusion

A time-dependent three-dimensional heat transfer model describing the flow field generated by the surface heated by an external radiation was developed. This model is applicable to the low Reynolds number flow in a microgravity environment. The results show a complex flow field generated by temperature gradients in the gas phase near the irradiated hot surface area. The induced flow appears like a source of flow slightly upstream from the center of the external radiation beam. Then, there is a sink of flow downstream when the hot gas stream cools by heat loss to the solid surface. Higher external radiant flux and a thermally thin solid enhance the induced flow and enlarge the heated gas region due to larger temperature gradients in the gas phase. Higher ambient flow velocity also generates more vigorous induced flow due to an increase in temperature gradient by compressing the heated flow stream toward the solid surface. Therefore, the heated gas region becomes smaller than that for lower ambient flow velocities, although the induced flow is increased.

Acknowledgments

This study is supported by the NASA Microgravity Science Program under Inter-Agency Agreement No. C-32000-R.

References

- Akita, K., 1978, "Ignition of Polymers and Flame Propagation on Polymer Surface," in: *Aspects of Degradation and Stabilization of Polymers*, H. H. G. Jellinek, ed., Elsevier Scientific, Chap. 10.
- Amos, B., and Fernandez-Pello, A. C., 1988, "Model of the Ignition and Flame Development on a Vaporizing Combustible Surface in a Stagnation Point Flow: Ignition by Vapor Fuel Radiation Absorption," *Combust. Sci. Tech.*, Vol. 62, pp. 331-343.
- Back, S. W., and Kim, J. S., 1991, "Ignition of a Pyrolyzing Solid With Radiatively Active Fuel Vapor," *Combust. Sci. Tech.*, Vol. 75, pp. 89-102.
- Brandrup, J., and Immergut, E. H., eds., 1975, *Polymer Handbook*, Wiley-Interscience, New York, Chap. 5.

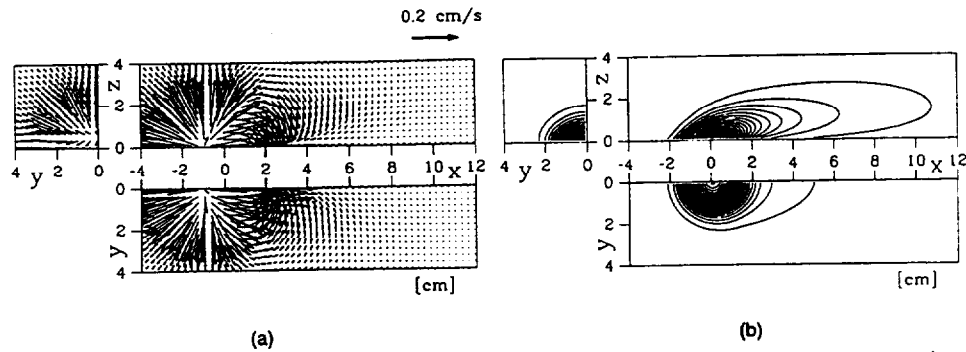


Fig. 10 (a) The distributions of velocity vector relative to ambient flow and (b) the temperature contours (from 310 K at the interval of 20 K) for the thermally thin solid ($\dot{q}_0 = 4 \text{ W/cm}^2$ and $u_\infty = 2 \text{ cm/s}$)

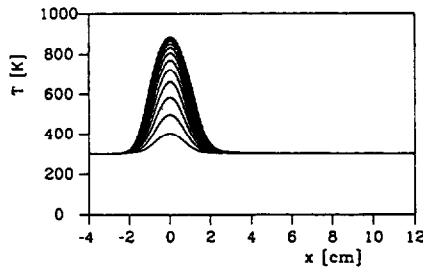


Fig. 11 Time history of the surface temperature distribution for the thermally thin solid at the interval of 0.5 s ($\dot{q}_0 = 4 \text{ W/cm}^2$ and $u_\infty = 2 \text{ cm/s}$)

- Kashiwagi, T., 1974, "A Radiative Ignition Model of a Solid Fuel," *Combust. Sci. Tech.*, Vol. 8, pp. 225-236.
- Kindelan, M., and Williams, F., 1977, "Gas-Phase Ignition of a Solid With In-Depth Absorption of Radiation," *Combust. Sci. Tech.*, Vol. 16, pp. 47-58.
- Kushida, G., Baum, H. R., Kashiwagi, T., and di Blasi, C., 1992, "Heat and Mass Transport From Thermally Degrading Thin Cellulosic Materials in a Microgravity Environment," *ASME JOURNAL OF HEAT TRANSFER*, Vol. 114, pp. 494-502.
- Mutoh, N., Hirano, T., and Akita, K., 1978, "Experimental Study on Radiative Ignition of Polymethylmethacrylate," *Seventeenth Symposium (International) on Combustion*, The Combustion Institute, Pittsburgh, PA, pp. 1183-1190.
- Olson, S. L., Ferkul, P. V., and Tien, J. S., 1988, "Near-Limit Flame Spread Over a Thin Solid Fuel in Microgravity," *Twenty-Second Symposium (International) on Combustion*, The Combustion Institute, Pittsburgh, PA, pp. 1213-1222.
- Olson, S. L., 1991, "Mechanisms of Microgravity Flame Spread Over a Thin Solid Fuel: Oxygen and Opposed Flow Effects," *Combust. Sci. Tech.*, Vol. 76, pp. 233-249.
- Van Dyke, M., 1964, *Perturbation Methods in Fluid Mechanics*, Academic Press, New York, pp. 149-158.

APPENDIX

A three-dimensional time-dependent heat transfer problem similar to the problem of interest is solved analytically to examine the accuracy of the numerical code used in this study. This problem is based on the Oseen flow. Then, the linearized energy equation is

$$\rho C_p \left\{ \frac{\partial T}{\partial t} + u_\infty \frac{\partial T}{\partial x} \right\} = k \Delta T \quad (\text{A1})$$

where T is the relative temperature with respect to an ambient temperature.

The initial condition is

$$\text{At } t = 0, \quad T = T_\infty$$

and boundary conditions are

$$\begin{aligned} \text{At } z = 0, \quad k \partial T / \partial z &= -\dot{q}(x, y) \\ \text{At } r = \infty, \quad T &= T_\infty \end{aligned}$$

where

$$\begin{aligned} \ddot{q} &= \frac{\dot{q}_0}{\pi} \exp\{-(r_p/r_0)^2\} \\ r_p^2 &= x^2 + y^2 \end{aligned}$$

Let

$$r = r_0 x(\bar{x}, \bar{y}, \bar{z}), \quad t = \frac{r_0}{u_\infty} \bar{t}$$

$$Pe_i = \frac{k}{\rho C_p r_0 u_\infty}$$

$$T - T_\infty = \frac{q_0 r_0}{k} \theta(\bar{x}, \bar{y}, \bar{z}, \bar{t})$$

Then, Eq. (A1) becomes

$$\frac{\partial \theta}{\partial \bar{t}} + \frac{\partial \theta}{\partial \bar{x}} = Pe_i \Delta \theta \quad (\text{A2})$$

We take the Laplace transformation of Eq. (A2) in time and then apply to the Fourier transformation in x and y . Then, Eq. (A2) becomes

$$\frac{d^2 \bar{\theta}(p, \xi, \eta, \bar{z})}{d\bar{z}^2} - \left\{ \xi^2 + \eta^2 + \frac{1}{Pe_i} (p + i\xi) \right\} \bar{\theta} = 0 \quad (\text{A3})$$

and boundary conditions are

$$\begin{aligned} \text{At } \bar{z} = \infty, \quad \bar{\theta} &= 0 \\ \text{At } \bar{z} = 0, \quad \bar{q}(\xi, \eta) &= \exp\{-(\xi^2 + \eta^2)/4\} \end{aligned}$$

The solution of Eq. (A3) with the above boundary conditions becomes

$$\bar{\theta} = \frac{\exp\left\{-\sqrt{(\xi^2 + \eta^2) + \frac{1}{Pe_i}(p + i\xi)} \bar{z}\right\} e^{-\frac{(\xi^2 + \eta^2)}{4}}}{p \sqrt{(\xi^2 + \eta^2) + \frac{1}{Pe_i}(p + i\xi)}} \quad (\text{A4})$$

We invert the Laplace transformation of the above solution using the convolution theorem and obtain the inverted solution

$$\begin{aligned} \theta^* &= \exp\left[\frac{-(\xi^2 + \eta^2)}{4}\right] \int_0^{\bar{t}} d\tau \sqrt{\frac{Pe_i}{\pi \tau}} \exp \\ &\quad \times \left[\frac{-\bar{z}^2}{4Pe_i \tau}\right] \exp[-\{Pe_i(\xi^2 + \eta^2) + i\xi\} \tau] \quad (\text{A5}) \end{aligned}$$

Next we proceed with Fourier inversion of Eq. (A5) to obtain the solution of Eq. (A1).

$$\theta = \int_0^{\bar{t}} \frac{\sqrt{Pe_i} \exp\{-(\bar{x} - \tau)^2 + \bar{y}^2\} / (1 + 4Pe_i \tau) - \bar{z}^2 / 4Pe_i \tau}{\pi^{3/2} \sqrt{\tau} (1 + 4Pe_i \tau)} d\tau \quad (\text{A6})$$